Energetic Properties of Magnetized Neutron Stars in General Relativity

Bobomurat Ahmedov

Ulugh Beg Astronomical Institute
Uzbekistan Academy of Sciences, Tashkent
National University of Uzbekistan, Tashkent

23 October 2020, RAGtime 22, Opava

PhD/postdoc under supervision of Zdenek

Habilitation DSc. thesis has been defended in 2016, more than 65 papers/WoS h-index > 22; The Best Young Researcher 2017 WoS Award; The Best Researcher in Engineering 2019 Scopus Award

Habilitation DSc. defended in 2019/more than 35 papers/The best young scientist of JINR, Dubna 2015; Award of the Czech Ministry of Education for the best young researcher 2018; Award of the Czech Physical Society for the best young researcher 2020

PhD study at Silesian University in Opava, Czech Republic

PhD thesis is defended in 2018/more than 25 papers/ WoS h-index > 14; Award of the Czech Physical Society for the best PhD thesis 2018; The Best Young Researcher 2019 Scopus


SIEMENS
Ingenuity for

Content

RAGtime 22 online


KAZAKHSTAN
ELEVATION :
2 000 m
1 500 m
1 000 m
500 m
200 m
0
Dzhusaly
Kzyl-Orda
(Ak Mechet)
Syr-Dar'ya
ARAL SEA
KARAKALPAKIA
Turkestan
Dzhambul
Chimkent
Tashauz
Urgench
UZBEKISTAN
Tashkent
Namangan
Syr-Dar'ya
Karadar'ya
Amudar'ya
Gulistan
Kokand
Andizhan
TURKMENISTAN
Bukhara
~350 km
KYRGYZ REPUBLIC
Samarkand
Kitab
Ashkhabad
Chardzhou
Dushanbe
IRAN
Mary
Kerki
TAJIKISTAN
0
200
400 km
Pyandzh
AFGHANISTAN
GRID-Arendal, 1998

GPS Stations by GFZ-Potsdam in Tashkent, Maidanak and Kitab

UN	AWESOME	Umran Inan	**Prof. Hans J. Haubold** *UN Office for Outer Space Affairs Vienna International Centre*
UNITED NATIONS	SUPERSID STANFORD SOLAR CENTER	Deborah Scherrer	

World SID & AWESOME Sites

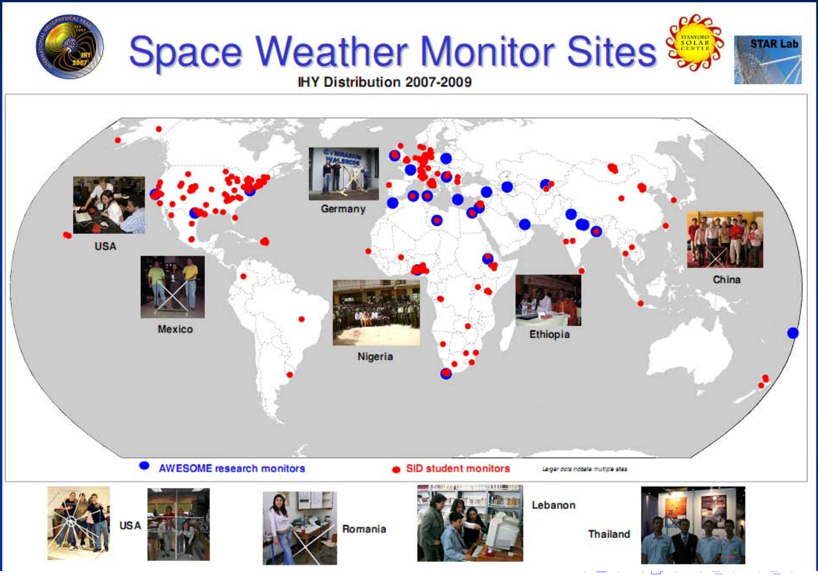

UzbekistanToday

Uzbekistan Intensifying the Work to Promote the Legacy of Mirzo Ulughbek, Astronomy and Aeronautics

Date Added: **15-09-2017**

Yesterday the President of Uzbekistan Shavkat Mirziyoyev signed the Resolution 'On the establishment of the Mirzo Ulughbek state specialized general boarding school and the Astronomy and Aeronautics Park.'

The boarding school with in-depth study of mathematics, astronomy, physics and informatics for 200 pupils and 150 places for students is created under the Astronomical Institute of the Academy of Sciences (the number of students in the future can be changed).

The Astronomical Institute has been instructed to ensure the participation of leading specialists in the school's educational process, in organizing lessons and practical exercises in astronomy using the available equipment.

The Astronomy and Aeronautics Park and the Planetarium as well as the boarding school will be located on the territory of the Astronomical Institute. Within the framework of the construction, it is planned to overhaul the main and historical buildings of the Institute, as well as pavilions of telescopes representing cultural and historical value.

The park will accommodate samples (models) of aircraft that are under the jurisdiction of the Ministry of Defense, the Uzbekistan Airways National Air Company and JSC Tashkent Mechanical Plant.

RAGtime 22 online

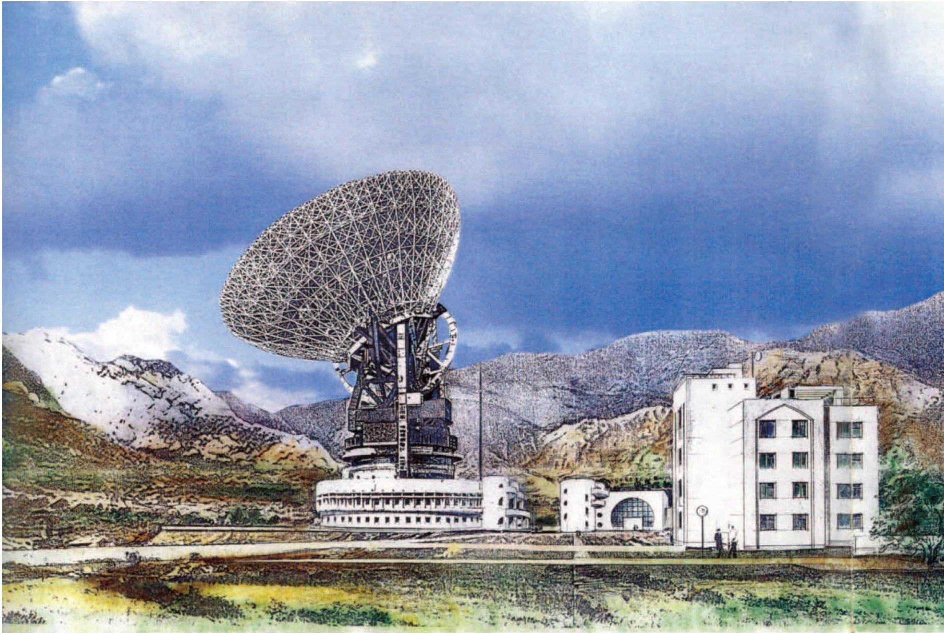

Test case: Kerr a=0.936

using 24h of observations

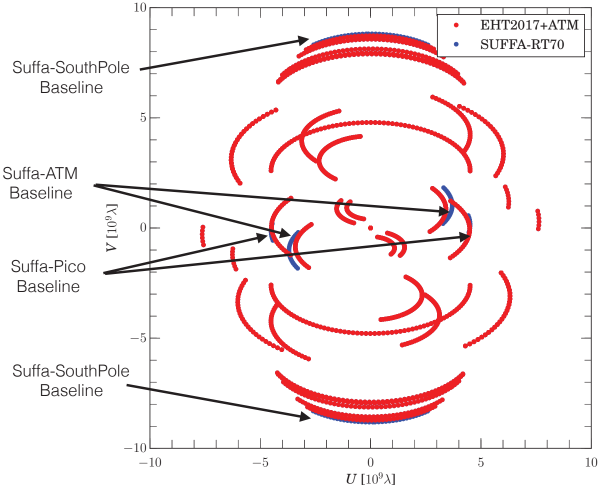

Test case: Kerr a=0.936

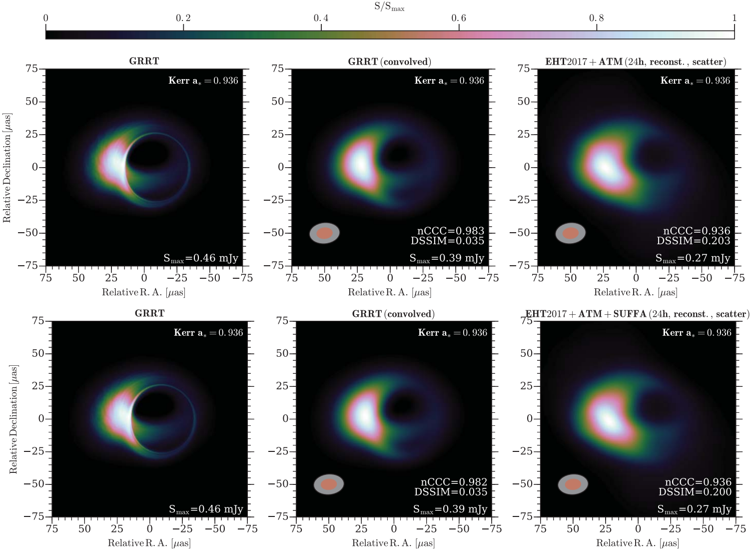

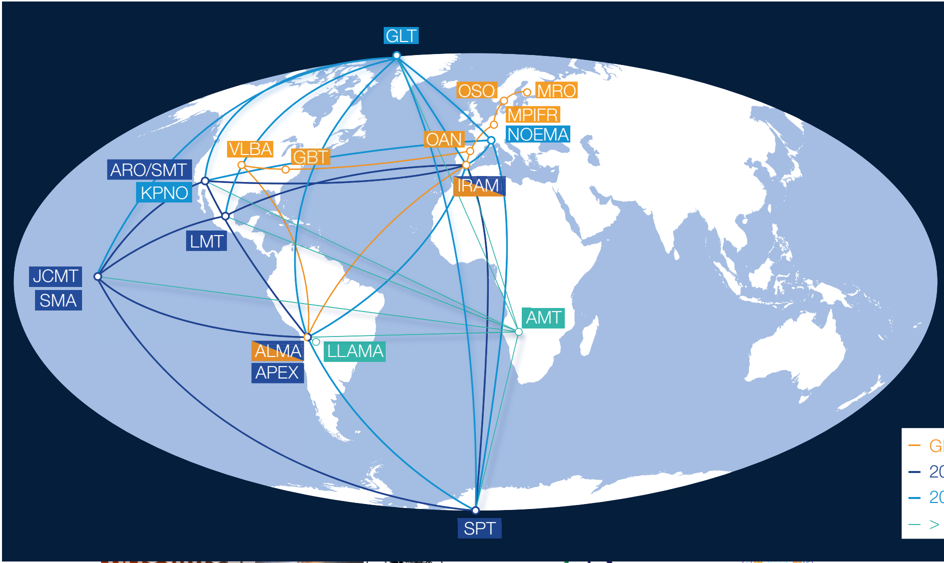
GLT
OSO
MRO
MPIFR
NOEMA
OAN
VLBA
GBT
ARO/SMT
KPNO
IRAM
LMT
JCMT
SMA
AMT
ALMA
LLAMA
APEX
SPT

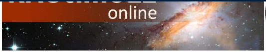
online

GRANDMA - Global Rapid Advanced Network Devoted to multimessenger addicts

20 observatories - 29 institutes/groups

PI. S. Antier (France)

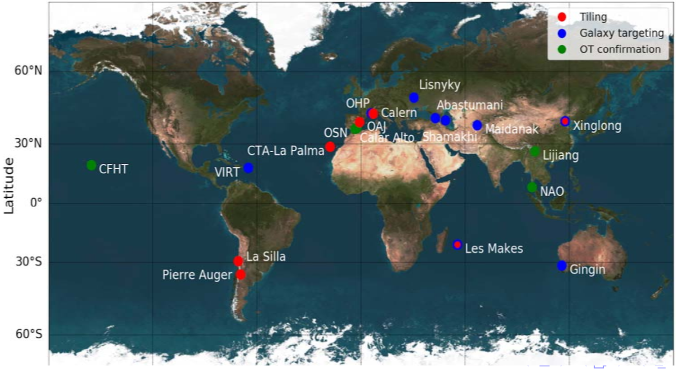

Maidanak observatory

- Participates in GRANDMA with two 60 cm telescopes – Nothern Zeiss-600 (NT) and Southern Zeiss-600 (ST)

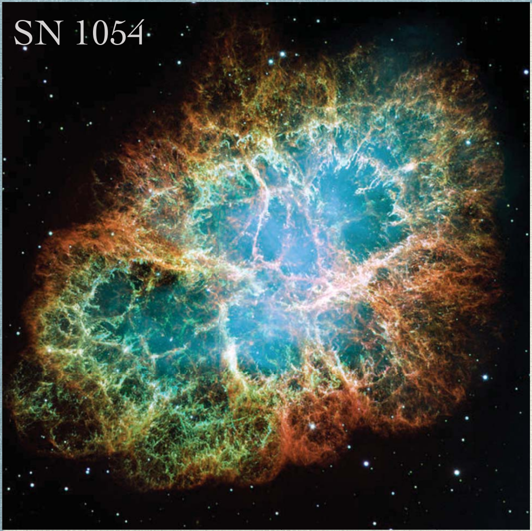

* Supernova explosions are spectacular events, marking the end of stellar life

* During maximum brightness, the supernova may briefly outshine an entire galaxy

* Before the development of the telescope, there have only been 5 supernovae seen in the last millennium

SN 1006 – Ibn Sina Supernova Record in Arabic

نارا خالصة ، ولا يكون لها برد مطفىء ، ولا أيضا تصعد صعودا سريعا ممعنا في حيز النار إلى أن تبلغ المكان الشديد قوة الذرية ، فيعرض لذلك أن يبقى التهابها واشتعالها مدة طويلة إما على صورة ذؤابة أو ذنب ، وأكثره شمالي وقد يكون جنوبيا ، وإما على صورة كوكب من الكواكب ، كالذي ظهر في سنة سبع وتسعين وثلاث مائة للهجرة ، فبقي قريبا من ثلاثة أشهر يلطف ويلطف حتى اضمحل ، وكان في ابتدائه إلى السواد والخضرة ، ثم جعل كل وقت يرمي بالشرر ويزداد بياضا ويلطف حتى اضمحل . وقد يكون على صورة لحية ، أو صورة حيوان له قرون ، وعلى سائر الصور ، وإنما يكون ذلك إذا كانت هناك مادة كثيفة واقفة ، تلطف أجزاؤها يسيرا يسيرا وتحلل عنه متصعدة كزوائد شعرية أو قرنية . ومنها المسماة أعتقا كأن تدويرها تشعير . وكل ما ثبت منها

---

(١) بالمدد : وبالمدد د ، سا || ف : ساقطة من ب ، ط (٢) كالموجودة : كالموجود د ، ط ، م (٣) ويحلقها غيرها : ويحلقه غيره ب ، د ، سا ، ط || موضعها : موضعه ب ، د ، سا ، ط .
(٥) في حقيقة : وحقيقة سا (٧) مقامه : مكانه د ، سا || يشتعل : ساقطة من د .
(٨) وخفيفة : خفيفة سا (٩) وخلصت : وحصلت سا . (١٠) وذات : ذات سا

Number of SN discoveries per year

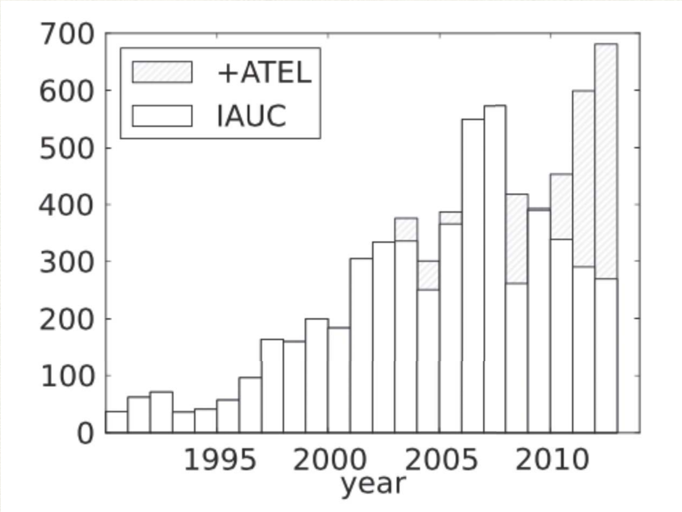

IAUC - International Astronomical Union Circulars
ATEL - The Astronomer's Telegram

Different types of core-collapse SNe

Type II -> H lines
Type I -> no H lines

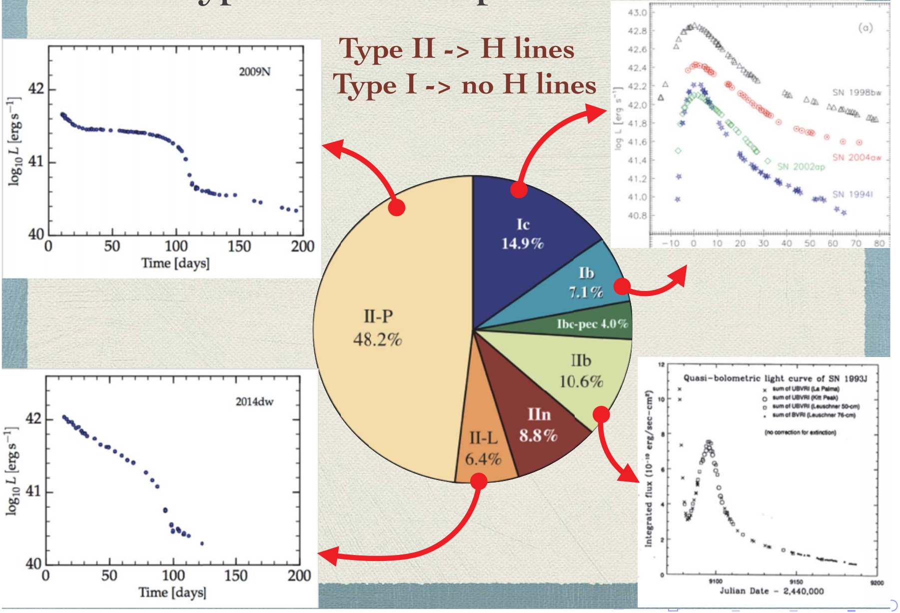

SN2017ein supernova

The supernova SN2017ein was discovered on 2017 May 25.99 (UT), in the nearby galaxy NGC 3938. It was observed on 25.77 (UT) at Maidanak observatory. Optical spectra obtained on May 26.6 (UT) indicated the supernova to be of Type Ic, about one week before maximum.

Reconstructing quasi-bolometric lightcurve

Bolometric correction to B-band *(Lyman et al. 2014)*

$$BC = -0.029 - 0.302\,(B - R) - 0.22\,(B - R)^2$$

Reconstructing quasi-bolometric lightcurve

Bolometric correction to B-band *(Lyman et al. 2014)*

$$BC = -0.029 - 0.302\,(B - R) - 0.22\,(B - R)^2$$

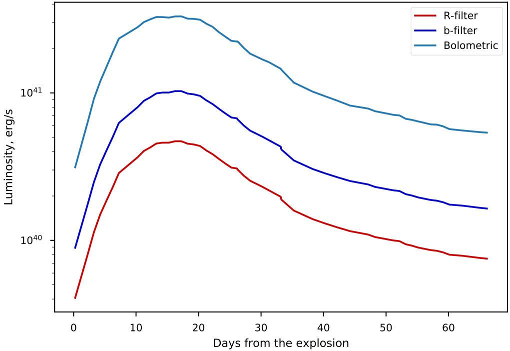

Fitting to the model

The model

- Photospheric phase, $t \leq 30$ days - *Arnett (1992)*
- Nebular phase, $t \geq 60$ days - *Sutherland, Wheeler (1984)*

Fitting to the model

The model

- Photospheric phase, $t \leq 30$ days - *Arnett (1992)*
- Nebular phase, $t \geq 60$ days - *Sutherland, Wheeler (1984)*

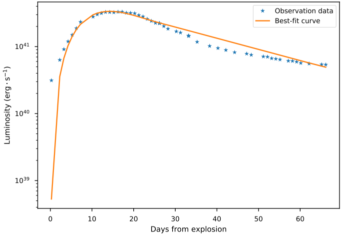

Fitting to the model

The model

- Photospheric phase, $t \leq 30$ days - *Arnett (1992)*
- Nebular phase, $t \geq 60$ days - *Sutherland, Wheeler (1984)*

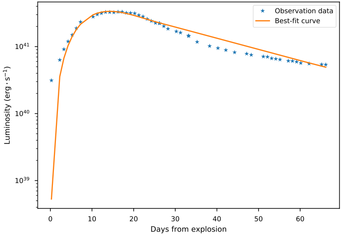

$M_{Ni} = 0.037 M_{\odot},\ M_{ej} = 1.246 M_{\odot},\ E_k = 1.641 \cdot 10^{51}$ **erg**

Content

RAGtime 22 online

Classical neutron stars

In 60s the first X-ray sources have been discovered.

They were neutron stars in close binary systems, BUT ...
.... they were «not recognized»....

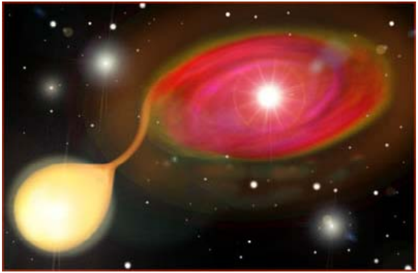

Now we know hundreds of X-ray binaries with neutron stars in the Milky Way and in other galaxies.

Accretion in close binaries

Accretion is the most powerful source of energy realized in Nature, which can give a huge energy output.

When matter fall down onto the surface of a neutron star up to 10 % of mc^2 can be released.

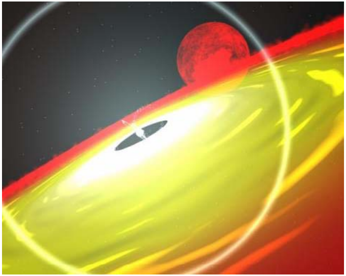

RAGtime 22

Zel'dovich *Sov. Phys. Dokl.* 9 195 (1964); Salpeter *Astrophys. J.* 140 796 (1964); Shakura & Sunyaev *Astron. Astrophys.* 24 337 (1973)

ENERGETICS

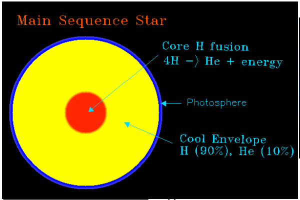

a few 10^{33} erg/s

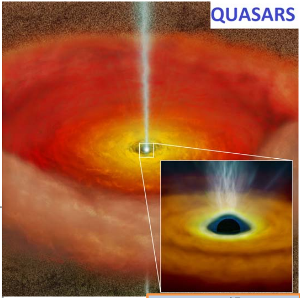

a few 10^{45} erg/s

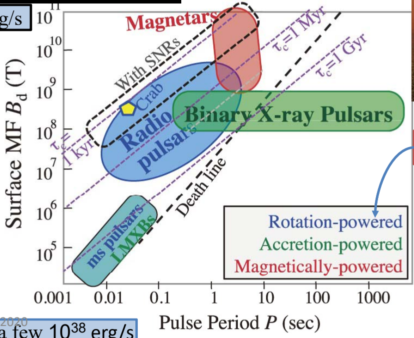

21 October 2020

a few 10^{38} erg/s

T.Gold,Nature,1968

Moreover, oscillating-powered pulsars/magnetars model has also been suggested and shown how oscillating kinetic energy transforms to EM radiation energy.

4

NSs

- RADIO PULSARS: 2000 discovered to date
- Radiate covering most of the electromagnetic spectrum
- Rotate with periods that span five decades (ms to a few hours)
- Are **powered** by their own rotational energy, residual surface heat or accretion
- Live tens of millions of years

29 magnetars: 15 SGRs (11 confirmed, 4 candidates), and 14 AXPs (12 confirmed, 2 candidate) discovered to date: http://www.physics.mcgill.ca/ pulsar/magnetar/main.html

- Magnetars are magnetically powered, rotating neutron stars
- Radiate almost entirely in X-rays, with luminosities 10^{33} to 10^{36} erg/s
- Emit typically brief (1-100 ms) bursts and very rarely, Giant Flares
- Rotate in a very narrow period interval (2-11 s) and slow down faster than any other object (10^{-10}-10^{-11} s/s^{-1})
- **Powered** by MF energy, which heats the NS and the surface glows persistently in X-rays, and fractures the crust inducing short, repeated bursts
- Die rather young; typical ages are 10 000 yrs

Radio pulsars

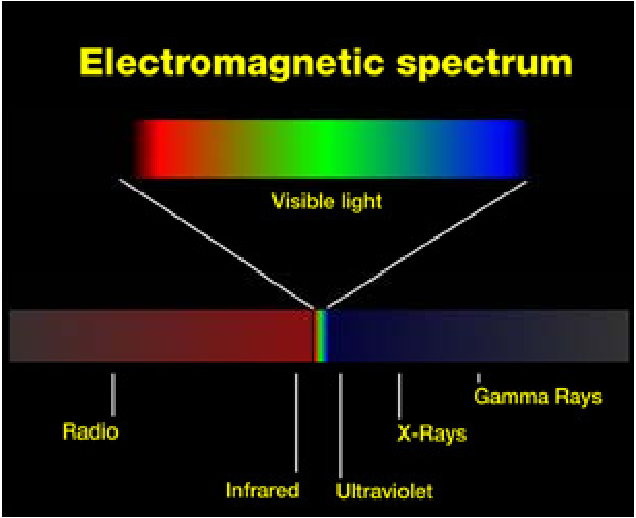

Magnetars

Magnetars

- $dE/dt > dE_{rot}/dt$
- By definition: The energy of the magnetic field is released

Magnetic fields 10^{14}–10^{15} G

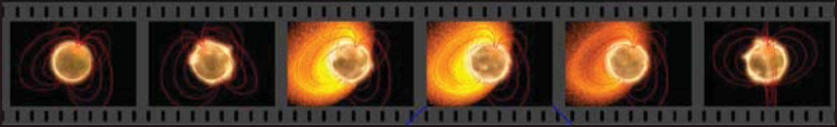

Gravitational collapse of the magnetized star

Due to conservation of magnetic flux during collapse

$$BR^2 = const \Rightarrow B = B_0 \left(R_0/R\right)^2$$

in the nonrelativistic limit magnetic moment $\mu \sim BR^3$ decays as

$$\mu = \mu_0 \left(R/R_0\right) \Rightarrow \lim_{R \to 0} \mu = 0 \ .$$

In GR during collapse magnetic moment decays as

$$\mu(t) = \mu_0 \left(4M^2/3R_0 ct\right) \ ,$$

and exterior magnetic field should decay with t^{-1} (Ginzburg & Ozernoy 1964, Anderson & Cohen 1970, Zeldovich & Novikov 1971).
The correct decay rate at late times of an initially static dipole electromagnetic radiation field outside a black hole is $t^{-(2l+2)}$ (Price 1972, Thorne 1971).

NS Magnetosphere

EF on the Star Surface:

$$E \propto \frac{\Omega R}{c} B \propto \frac{\Omega \xi}{c} B \propto 10^{10} \mathrm{V} \cdot \mathrm{cm}^{-1}$$

Goldreich & Julian, 1969, Astrophys.J, 157, 869

Cascade generation of electron-positron plasma leads to formation of MS with plasma screening longitudinal EF.

Plasma is corotating with the neutron star.

Charges along open field lines create plasma modes.

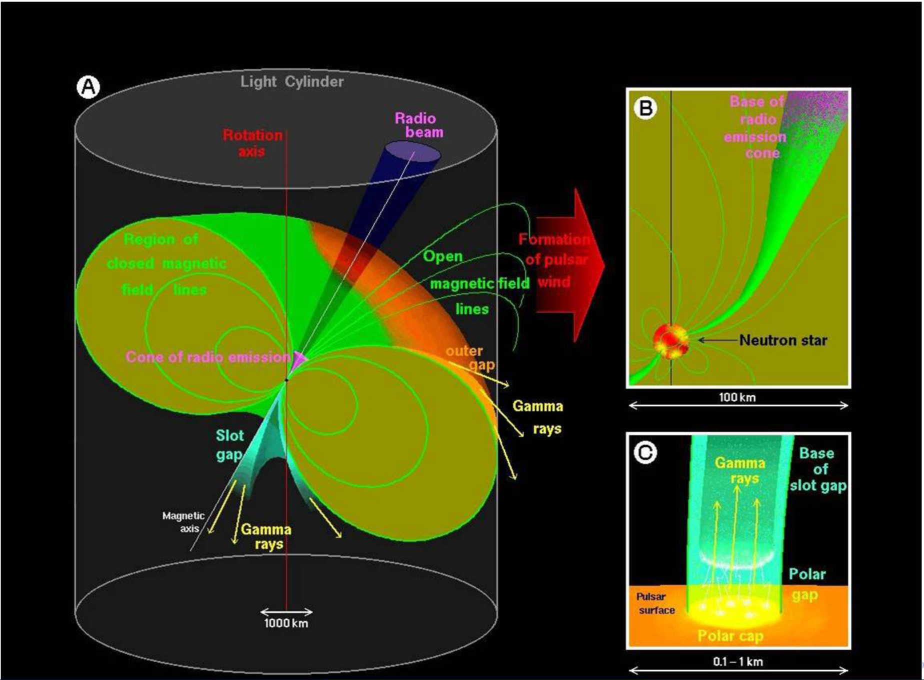
A
Light Cylinder
Radio beam
Rotation axis
Region of closed magnetic field lines
Open magnetic field lines
Formation of pulsar wind
Cone of radio emission
outer gap
Gamma rays
Slot gap
Magnetic axis
Gamma rays
1000 km
B
Base of radio emission cone
Neutron star
100 km
C
Gamma rays
Base of slot gap
Polar gap
Pulsar surface
Polar cap
0.1 – 1 km

Oscillating NSs

- NSs are endowed with intense EM fields, but they are also subject to oscillations of various type.
- Evidence for stellar oscillations coming from the observation of QPOs following giant flares of SGRs (Israel et al., 2005; Strohmayer & Watts, 2005; Watts & Strohmayer, 2006, 2007).
- The study of internal structure of NSs is of great importance for fundamental physics because matter inside NS is under extreme conditions. The study of proper oscillations of isolated NSs may provide an opportunity to obtain important information about the internal structure of these objects.

Model Assumptions

Difficulty of simultaneously solving the Maxwell eqs

$$3!F_{[\alpha\beta,\gamma]} = 2\left(F_{\alpha\beta,\gamma} + F_{\gamma\alpha,\beta} + F_{\beta\gamma,\alpha}\right) = 0\ , \qquad F^{\alpha\beta}{}_{;\beta} = 4\pi J^{\alpha}\ ,$$

and the highly nonlinear Einstein eqs

$$R_{\alpha\beta} - \frac{1}{2}g_{\alpha\beta}R = \kappa T_{\alpha\beta}\ , \quad T_{\alpha\beta} = T_{(G)\alpha\beta} + T_{(em)\alpha\beta}\ .$$

E/M Fields are considered in a given background Geometry: Very Good Approximation

$$T_{(G)\alpha\beta} \gg T_{(em)\alpha\beta}\ , T_{\alpha\beta} \approx T_{(G)\alpha\beta}\ .$$

Model Assumptions

MF does not contribute to the total energy momentum

$$\frac{B^2}{8\pi\langle\rho_0\rangle c^2} \simeq 1.6\times 10^{-6}\left(\frac{B}{10^{15}\ \mathrm{G}}\right)^2\left(\frac{1.4\ M_\odot}{M}\right)\left(\frac{R}{15\ \mathrm{Km}}\right)^3 .$$

Space-time metric

$$ds^2 = -e^{2\Phi(r)}dt^2 + e^{2\Lambda(r)}dr^2 - 2\omega(r)r^2\sin^2\theta dt d\phi + r^2 d\theta^2 + r^2\sin^2\theta d\phi^2 .$$

$\omega(r)$ is the Lense-Thirring angular velocity and outside the star is given by

$$\omega(r) \equiv \frac{d\phi}{dt} = -\frac{g_{0\phi}}{g_{\phi\phi}} = \frac{2J}{r^3} .$$

$N \equiv (1-2M/r)^{1/2}$ is lapse function, $\omega_{\rm LT} = 2aM/r^3$ is the Lense-Thirring angular velocity, R is the star radius, $\eta = r/R$ is the dimensionless radial coordinate, $\varepsilon = 2M/R$ is the compactness parameter, $\beta = I/I_0$ is the moment of inertia of the star in units of $I_0 = MR^2$ and $\kappa = \varepsilon\beta$.

Model Assumptions

Velocity perturbation

$$\delta u^\alpha = \Gamma\left(1, \delta v^i\right) = \Gamma\left(1, e^{-\Lambda}\delta v^{\hat{r}}, \frac{\delta v^{\hat{\theta}}}{r}, \frac{\delta v^{\hat{\phi}}}{r\sin\theta}\right) .$$

For small velocity perturbations $\delta v^i/c \ll 1$:

$$\Gamma = \left[-g_{00}\left(1 + g_{ik}\frac{\delta v^i \delta v^k}{g_{00}}\right)\right]^{-1/2} \simeq e^{-\Phi} .$$

Toroidal Oscillations

$$\delta v^{\hat{i}} = \left\{0, \frac{1}{\sin\theta}\partial_\phi Y_{\ell' m'}(\theta,\phi) , -\partial_\theta Y_{\ell' m'}(\theta,\phi)\right\}\eta(r)\mathrm{e}^{-\mathrm{i}\omega t} .$$

Frequency range for small velocity perturbations

$$\omega\bar{\xi} \ll c , \quad \bar{\xi} \approx 10^{-3}R = 10^{3}\mathrm{cm} , \quad \omega \ll 3\times 10^{7}\mathrm{Hz} .$$

Toroidal Oscillations

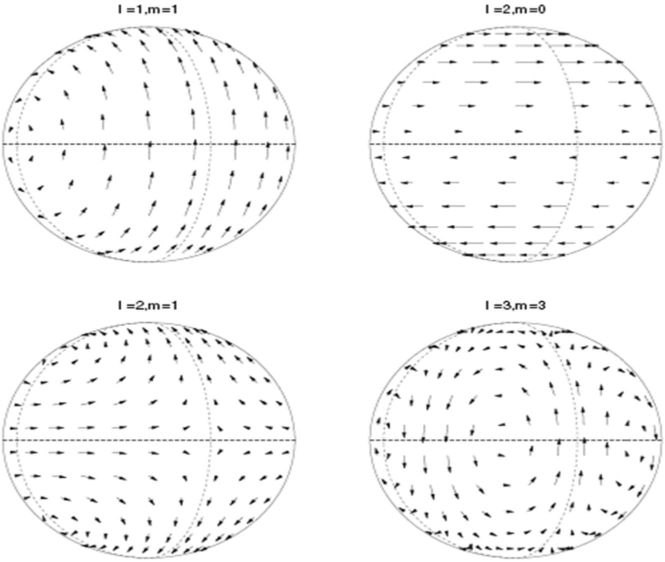

Content

RAGtime 22 online

Content

RAGtime 22 online

GR Effects in Pulsar MS

Goldreich-Julian charge density

$$\rho_{GJ} = -\frac{\Omega B_0}{2\pi c}\frac{1}{N\eta^3}\frac{f(\eta)}{f(1)}\left\{1-\frac{\kappa}{\eta^3}-L\left(1-\frac{\varepsilon}{\eta}\right)\frac{1}{\eta^2}\frac{4\sin^2\frac{\theta}{2}}{\sin^2\theta}\right\} .$$

Charge density ρ is proportional to MF with the proportionality coefficient being constant along the given MF line

$$\rho = \frac{\Omega B_0}{2\pi c}\frac{1}{N\eta^3}\frac{f(\eta)}{f(1)}A(\xi) ,$$

where $\xi = \theta/\Theta$, and polar angle Θ of the last open magnetic line

$$\Theta \cong \sin^{-1}\left\{\left[\eta\frac{f(1)}{f(\eta)}\right]^{1/2}\sin\Theta_0\right\} , \quad \Theta_0 = \sin^{-1}\left(\frac{R}{R_{LC}f(1)}\right)^{1/2} ,$$

Muslimov & Tsygan (1990, 1992), Beskin (1990), Muslimov & Harding (1997)

GR Effects in Pulsar MS

EF $E_{||}$ is

$$E_{||} = -E_{vac}\Theta_0^2 \frac{3(\kappa - L\varepsilon)}{2\eta^4}(1 - \xi^2) \ ,$$

where $E_{vac} \equiv (\Omega R/c)B_0$.

The ratio of polar-cap energy losses

$$\frac{(L_p)_{max}}{(L_p)_{max \ (l=0)}} = 1 - \frac{L(\kappa + \varepsilon - 2\kappa\varepsilon)}{\kappa(1-\kappa)} + \frac{L^2\varepsilon(1-\varepsilon)}{\kappa(1-\kappa)} \ .$$

V. S. Morozova, B. J. Ahmedov and V. G. Kagramanova, General Relativistic Effect of Gravitomagnetic Charge on Pulsar Magnetosphere and Particle Acceleration in a Polar Cap, **ApJ**, 2008, V 684, 1359.

GJ charge density for slowly rotating and oscillating NS

$$\rho_{\rm GJ} = -\frac{\Omega B_0}{2\pi c}\frac{1}{\alpha \bar{r}^3}\frac{f(\bar{r})}{f(1)}\left(1-\frac{\kappa}{\bar{r}^3}\right) - \frac{1}{4\pi c}\frac{1}{R\bar{r}^4}\frac{B_0 e^{-i\omega t}}{\Theta^2(\bar{r})}\frac{1}{N}\frac{f(\bar{r})}{f(1)}\tilde{\eta}(\bar{r})l'(l'+1)Y_{l'm'} \ .$$

Using small angles θ approximation

$$Y_{l'm'}(\theta,\phi) \approx A_{l'm'}(\phi)\theta^m \ ,$$

one could get the ratio $\delta\rho_{\rm GJ\ l'm'}/\rho_{\rm GJ,0}$ in the form

$$\delta\rho_{\rm GJ\ l'm'}/\rho_{\rm GJ,0} = \frac{K}{2\bar{r}^{2-m/2}}\Theta_0^{m-2}\left(\frac{f(\bar{r})}{f(1)}\right)^{\frac{2-m}{2}}\frac{l'(l'+1)A_{l'm'}(\phi)}{\left(1-\frac{\kappa}{\bar{r}^3}\right)} \ ,$$

where $K=\tilde{\eta}(1)/\Omega R$.

Ratio $\delta\rho_{\rm GJ\ l'm'}/\rho_{\rm GJ,0}$ for the mode $(1,0)$ (left-hand top panel), $(1,1)$ (left-hand bottom panel), $(2,0)$ (right-hand top panel) and $(2,1)$ (right-hand bottom panel). NS parameters $\kappa = 0.15$, $\varepsilon = 1/3$, $K = 0.01$, $\Theta_0 = 0.008$, $\Omega = 1{\rm rad\ s}^{-1}$.

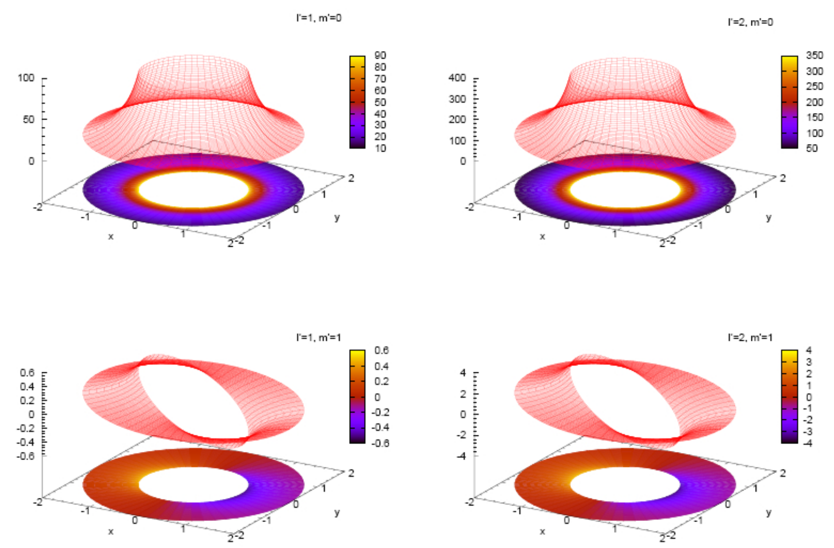

Ratio of longitudinal component of EF to E_0 for the mode $(1,0)$ (left-hand top panel), $(1,1)$ (left-hand top panel), $(2,0)$ (right-hand top panel) and $(2,1)$ (right-hand bottom panel).

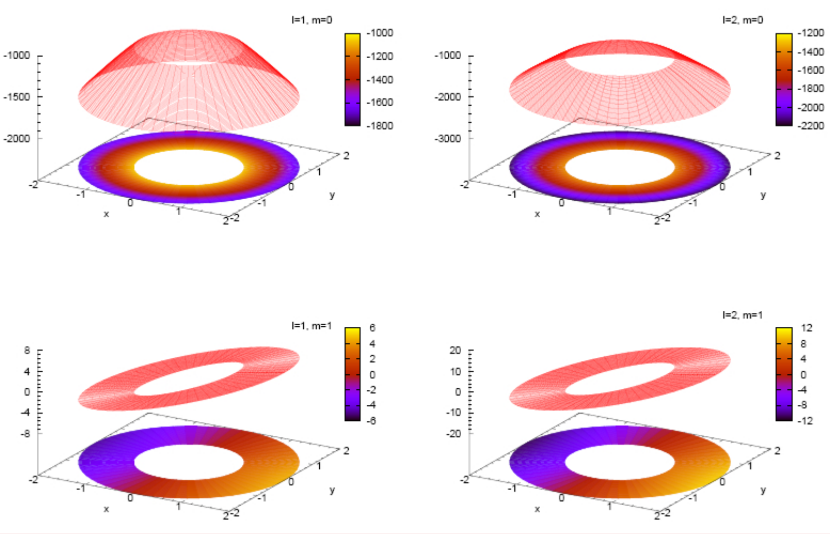

Energy losses of slowly rotating and oscillating NS

$$
\begin{aligned}
L_{|m\neq 0} &= R^3 N_R B_0^2 \Bigg| \Bigg\{ \frac{\Omega^2 R}{2cN_R}(1-\kappa)^2 \frac{\Theta_0^4}{4} \\
&+ \frac{\Omega}{4c}\frac{1}{N_R}(1-\kappa)\tilde{\eta}(1) l(l+1) A_{lm} \frac{\Theta_0^{m+4}}{m+4} \\
&- \frac{\Omega}{2c}\frac{1}{N_R}(1-\kappa) A_{lm}\tilde{\eta}(1) \frac{\Theta_0^{m+2}}{m+2} \\
&- \frac{1}{2c}\frac{1}{RN_R} A_{lm}^2 \tilde{\eta}^2(1) l(l+1) \frac{\Theta_0^{2m+2}}{2m+2} \Bigg\} \Bigg|
\end{aligned}
$$

and

$$
\begin{aligned}
L_{|m=0} &= R^3 N_R B_0^2 \frac{\Theta_0^4}{8} \Bigg| \left[\Omega R(1-\kappa) - A_{l0}\tilde{\eta}(1)\right] \Bigg\{ \frac{\Omega}{cN_R}(1-\kappa) \\
&+ \frac{1}{2c}\frac{1}{N_R}\tilde{\eta}(1) l(l+1) A_{l0} \Bigg\} \Bigg| .
\end{aligned}
$$

The ratio L_m/L_{rot} as a function of parameter $K = \tilde{\eta}(1)/\Omega R$ for modes $(1,1)$ (continuous red line) and $(2,1)$ (dotted blue line).

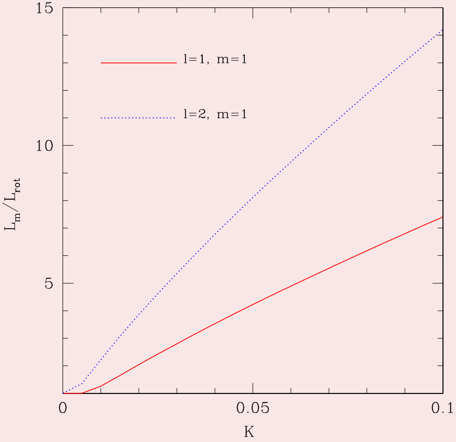

Constrains on parameters of Einstein-Aether gravity

Radio-load isolated NSs

P. A. Caraveo, Annual Review of Astronomy and Astrophysics, (2014)

Neutron star	Period, P millisecond	$\frac{dP}{dt} \times 10^{-15}\ s/s$	c_{13}, (c_{14}=0) ICS	c_{14}, (c_{13}=0) ICS	c_{13}, (c_{14}=0) CR	c_{14}, (c_{13}=0) CR
PSR J1057 – 52269	197.114	5.83	0.952158	-39.8041	0.98342	-42.3326
PSR J1509 – 5850	88.925	9.17	0.951734	-39.4366	0.98658	-41.6524
PSR J1952 + 3252	39.534	5.83	0.951968	-39.9528	0.98698	-42.1368
PSR J2030 + 3641	200.129	6.51	0.952169	-39.8139	0.97986	-43.0021
PSR J2043 + 2740	96.131	1.23	0.952085	-39.7405	0.97963	-43.0124

13

Radio-quite isolated NSs

S.Mereghetti, Astrophysics and Space Science 2011

Neutron star	Period, P millisecond	$\frac{dP}{dt} \times 10^{-15}$ s/s	c_{13}, (c_{14}=0) ICS	c_{14}, (c_{13}=0) ICS	c_{13}, (c_{14}=0) CR	c_{14}, (c_{13}=0) CR
PSR J1746 − 3239	199.541	6.56	0.952171	-39.8153	0.98465	-42.6547
PSR J0106 + 4855	83.157	0.428	0.951896	-39.3827	0.98015	-43.0154
PSR J1836 + 5925	173.264	1.5	0.951938	-39.3482	0.98652	-43.65812
PSR J2028 + 3332	176.707	4.86	0.952156	-39.8026	0.9845	-42.6895
PSR J2139 + 4716	282.849	1.8	0.951767	-39.4654	0.98432	-43.0098
PSR J2030 + 4415	227.070	6.49	0.952144	-39.7917	0.98654	-42.3651
PSR J1957 + 5033	374.806	6.83	0.952022	-39.6858	0.97986	-42.3651
PSR J2055 + 2539	319.561	4.11	0.95196	-39.6324	0.9814	-41.9856

14

Content

RAGtime 22 online

Part time (Intermittent) pulsars (PSR 1931+24)

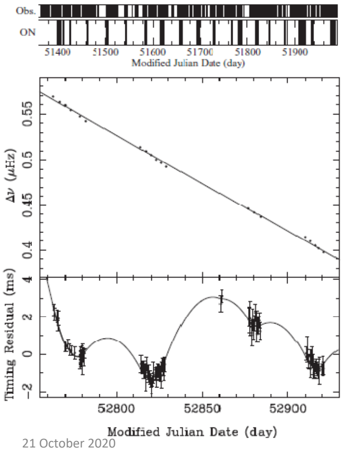

Kramer et.al, Nature, 2006

- Only visible for 20 % of time
- ON period 5-10 days
- OFF period 25-35 days
- Spin period 813ms
- Distance 4,6 kpc

$$\dot{\nu}_{ON} = -16.3 \times 10^{-15} Hz/s$$

$$\dot{\nu}_{OFF} = -10.8 \times 10^{-15} Hz/s$$

Bing Zhang et.al MNRAS 2006

REACTIVATED DEAD PULSAR

21 October 2020 8

More intermittent pulsars

Properties: J1832+0031

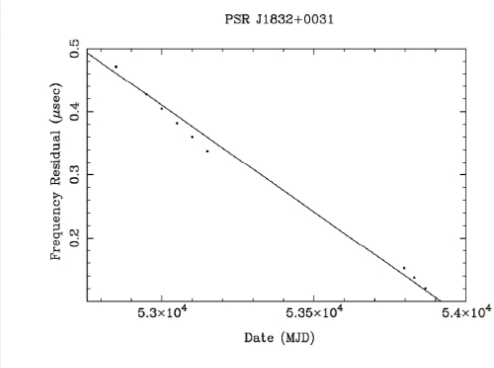

- 'on' state >300 days
- 'off' state ~700 days
- Quasi-periodicity ?
- Increase in slow-down rate during 'on' state similar to B1931+24

Possible explanations

- **Nulling?** (Backer (1970))

  Nulling phenomenon lasts only for a few pulse periods and not on a time-scales of tens of days

- **Precession?**

  Cannot produce a transition from the ON to the OFF state in less than 10 s

- **Global failure of charge particles currents in the magnetosphere?** (Lyne (2009), Gurevich&Istomin (2007))

  Lack of a physical mechanism for changing the plasma flow in the magnetosphere in such a drastic way

There is no self-consistent explanation of the phenomena yet

Transition from the OFF to the ON state of intermittent pulsar could correspond to the reactivation of a 'dead' pulsar above 'death line' (Zhang, Gil & Dyks, 2007)

Death line is the $P - \dot{P}$ or $P - B$ diagram which indicates the region where pulsar can support radio emission from magnetosphere (Kantor, Tsygan, 2004).

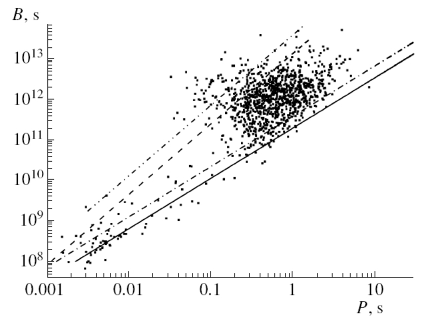

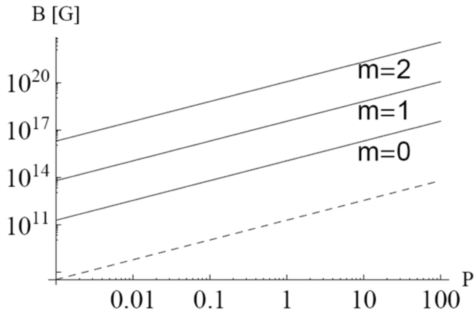

Ahmedov B.J., Morozova V.S. Plasma Magnetosphere Formation Around Oscillating Magnetized Neutron Stars, **ApSS**, 2009, V. 319, 115

Damping times of toroidal modes for a neutron star

Mode	ν (kHz) (1)	$E_{\rm T}$(erg) (2)	$L_{\rm em}^{\rm Newt}$(erg s^{-1}) (3)	$L_{\rm em}^{\rm GR}$(erg s^{-1}) (4)	$\tau_{\rm gw}(s)$ (5)	$\tau_{\rm em}^{\rm Newt}(s)$ (6)	$\tau_{\rm em}^{\rm GR}(s)$ (7)	$\tau_{\rm gw}/\tau_{\rm em}^{\rm GR}$ (8)	$\tau_{\rm em}^{\rm Newt}/\tau_{\rm em}^{\rm GR}$ (9)
${}_1t_1$	17.9	1.09×10^{49}	1.77×10^{43}	1.57×10^{44}	...	1.23×10^{6}	1.39×10^{5}	...	8.85
${}_1t_2$	30	6.40×10^{48}	1.44×10^{44}	1.28×10^{45}	...	8.88×10^{4}	1.00×10^{4}	...	8.88
${}_1t_3$	43	1.59×10^{48}	5.98×10^{44}	5.30×10^{45}	...	5.32×10^{3}	6.00×10^{2}	...	8.87
${}_1t_4$	52.7	2.72×10^{47}	1.33×10^{45}	1.18×10^{46}	...	4.08×10^{2}	4.60×10^{1}	...	8.87
${}_2t_0$	0.36	3.31×10^{47}	6.86×10^{32}	3.45×10^{33}	6.62×10^{11}	9.65×10^{14}	1.92×10^{14}	3.45×10^{-3}	5.03
${}_2t_1$	17.9	3.26×10^{49}	9.32×10^{42}	4.96×10^{43}	7.60×10^{5}	7.00×10^{6}	1.31×10^{6}	0.58	5.34
${}_2t_2$	30	1.92×10^{49}	2.17×10^{44}	1.15×10^{45}	2.33×10^{5}	1.77×10^{5}	3.33×10^{4}	70	5.32
${}_2t_3$	43	4.76×10^{48}	1.83×10^{45}	9.72×10^{45}	1.51×10^{4}	5.21×10^{3}	9.79×10^{2}	15.43	5.32
${}_2t_4$	52	8.15×10^{47}	6.10×10^{45}	3.24×10^{46}	4.68×10^{3}	2.67×10^{2}	5.03×10^{1}	93.04	5.31

Damping times of spheroidal modes for a neutron star

Mode	ν (kHz) (1)	$E_{\rm T}$(erg) (2)	$L_{\rm em}^{\rm Newt}$(erg s^{-1}) (3)	$L_{\rm em}^{\rm GR}$(erg s^{-1}) (4)	$\tau_{\rm gw}(s)$ (5)	$\tau_{\rm em}^{\rm Newt}(s)$ (6)	$\tau_{\rm em}^{\rm GR}(s)$ (7)	$\tau_{\rm gw}(s)/\tau_{\rm em}^{\rm GR}(s)$ (8)	$\tau_{\rm em}^{\rm Newt}/$ (9)
${}_2p_2$	104.72	1.55×10^{50}	9.04×10^{44}	4.56×10^{45}	0.23×10^{-3}	3.43×10^{5}	6.79×10^{4}	0.34×10^{-6}	4.4
${}_2f$	28.56	1.59×10^{52}	2.38×10^{43}	7.41×10^{44}	7.50×10^{-3}	1.34×10^{9}	4.29×10^{7}	1.75×10^{-10}	31.24
${}_2s_2$	14.61	2.53×10^{53}	4.46×10^{43}	1.03×10^{45}	1×10^{4}	1.13×10^{10}	4.90×10^{8}	0.2×10^{-4}	23.06
${}_2s_1$	8.6	1.32×10^{54}	5.13×10^{43}	1.12×10^{45}	4.32×10^{4}	5.15×10^{10}	2.36×10^{9}	1.83×10^{-5}	21.82
${}_2i_2$	0.63	4.08×10^{47}	5.49×10^{43}	1.16×10^{45}	5.04×10^{9}	1.48×10^{4}	7.01×10^{2}	0.72×10^{7}	21.11
${}_2i_1$	0.35	1.63×10^{53}	5.49×10^{43}	1.16×10^{45}	8.64×10^{5}	5.93×10^{9}	2.80×10^{8}	3.1×10^{-3}	21.18
${}_2g_2^s$	0.12	5.49×10^{43}	5.49×10^{43}	1.16×10^{45}	7.57×10^{16}	5.24×10^{-3}	2.47×10^{-4}	3.1×10^{20}	21.21
${}_2g_3^s$	0.1	1.96×10^{40}	5.49×10^{43}	1.16×10^{45}	1.17×10^{17}	0.71×10^{-3}	0.34×10^{-4}	3.4×10^{21}	20.88

Alternative idea for the explanation of part time pulsars phenomena

- During the ON state pulsar is oscillating: stellar oscillations create relativistic wind of charged particles by virtue of additional accelerating electric field
- In a period of about 10 days the stellar oscillations are damped and the OFF period starts
- Quasi-periodic stellar glitches excite oscillations again, thus, being responsible for the emergence of new ON states with a certain periodicity

online

Scheme for part-time pulsar model

Deathline for radio pulsars shifts up due to negative deformation, and limited by lower limit for the deformation parameter.

Schematic view for to explain the nature of part-time pulsars by time dependence of their deformation

$$L(t) = f\big(\epsilon(t)\big) \rightarrow \epsilon(t) = f^{*}\big(L(t)\big)$$

from observational data for ON and OFF states

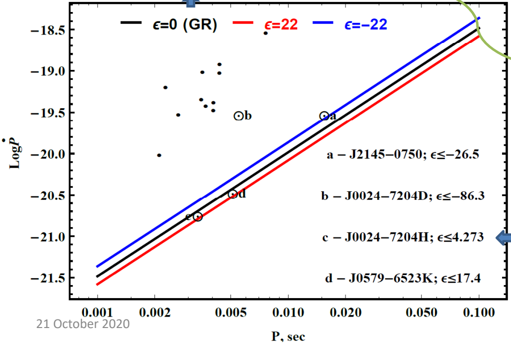

Fitting function for deformation parameter taking account the lower limit.

21 October 2020

9

Content

Plasma magnetosphere of NS

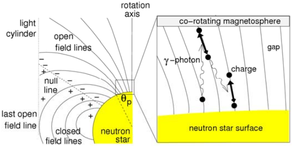

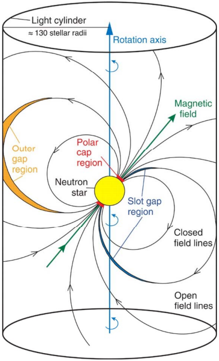

Goldreich & Julian 1969

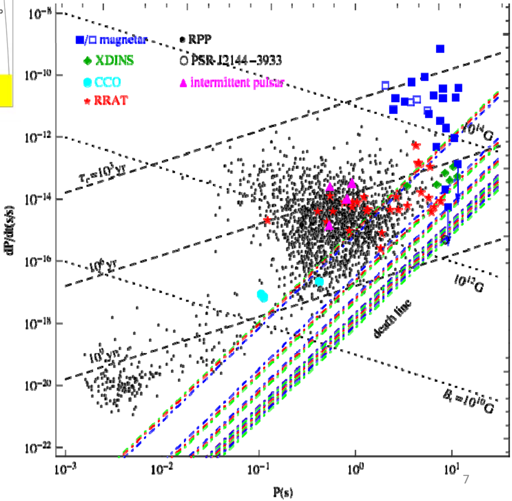

Relativistic death line for magnetars

- **The activity of magnetars is observed in the form of bursts in X-ray and γ-ray bands, while there is no periodic radio emission from the majority of magnetars in the same range of frequencies of ordinary pulsars.**
- **The absence of radio emission from magnetars is related to their slow rotation, i.e. the low energy of the primary particles, accelerated near the surface of the star.**
- **The death-line for magnetars, i.e. the line in the $P - \dot{P}$ diagram that separates the regions where the neutron star may be radio-loud or radio-quiet.**
- **We consider the influence of magnetar oscillations on the conditions for the radio emission generation in the MS of magnetars and revisit the problem of magnetars death-line, by taking into account the role both of rotation and of toroidal oscillations in a relativistic framework.**

Relativistic death line for magnetars

- **The activity of magnetars is observed in the form of bursts in X-ray and γ-ray bands, while there is no periodic radio emission from the majority of magnetars in the same range of frequencies of ordinary pulsars.**
- **The absence of radio emission from magnetars is related to their slow rotation, i.e. the low energy of the primary particles, accelerated near the surface of the star.**
- **The death-line for magnetars, i.e. the line in the $P - \dot{P}$ diagram that separates the regions where the neutron star may be radio-loud or radio-quiet.**
- **We consider the influence of magnetar oscillations on the conditions for the radio emission generation in the MS of magnetars and revisit the problem of magnetars death-line, by taking into account the role both of rotation and of toroidal oscillations in a relativistic framework.**

Relativistic death line for magnetars

- **The activity of magnetars is observed in the form of bursts in X-ray and γ-ray bands, while there is no periodic radio emission from the majority of magnetars in the same range of frequencies of ordinary pulsars.**
- **The absence of radio emission from magnetars is related to their slow rotation, i.e. the low energy of the primary particles, accelerated near the surface of the star.**
- **The death-line for magnetars, i.e. the line in the $P - \dot{P}$ diagram that separates the regions where the neutron star may be radio-loud or radio-quiet.**
- **We consider the influence of magnetar oscillations on the conditions for the radio emission generation in the MS of magnetars and revisit the problem of magnetars death-line, by taking into account the role both of rotation and of toroidal oscillations in a relativistic framework.**

Relativistic death line for magnetars

- **The activity of magnetars is observed in the form of bursts in X-ray and γ-ray bands, while there is no periodic radio emission from the majority of magnetars in the same range of frequencies of ordinary pulsars.**
- **The absence of radio emission from magnetars is related to their slow rotation, i.e. the low energy of the primary particles, accelerated near the surface of the star.**
- **The death-line for magnetars, i.e. the line in the $P - \dot{P}$ diagram that separates the regions where the neutron star may be radio-loud or radio-quiet.**
- **We consider the influence of magnetar oscillations on the conditions for the radio emission generation in the MS of magnetars and revisit the problem of magnetars death-line, by taking into account the role both of rotation and of toroidal oscillations in a relativistic framework.**

The critical magnetic field is defined as $B_c = m^2c^3/e\hbar \approx 4.414 \times 10^{13}\mathrm{G}$, where m is the electron mass and e is the electron charge.

When distance between two neighboring Landau levels becomes equal to the rest energy of the electron $\hbar\omega_c = mc^2$, $\omega_c = eB_c/mc$.

Characteristic energy of the curvature gamma quanta is $\epsilon_\gamma \approx \hbar c\gamma^3/R_c$.

Dependence of death-lines from parameter κ

When $\chi = 0$ the value of the magnetic field for which the generation of secondary plasma still possible is

$$B_0 \gtrsim \left(\frac{\kappa}{f(1)}\right)\left(\frac{P}{1\mathrm{s}}\right)^{7/3}\left(\frac{R_s}{10\mathrm{km}}\right)^{-3} 10^{12}\mathrm{G}\ ,$$

which gives the expression for the death-line of the magnetars in the form

$$\log \dot{P} = \frac{11}{3}\log P - 15.6 - 2\log\left(\frac{\kappa}{f(1)}\right) - 6\log\left(\frac{R_s}{10\mathrm{km}}\right)\ .$$

Death-lines for the aligned magnetar for different values of the parameter κ. The dashed line indicates the position of the Newtonian death-line. Crosses and squares indicate the position of SGRs and AXPs, respectively. AXPs from which the radio emission has been registered are marked with ticks, radio-loud soft gamma-ray repeater is enclosed in circle.

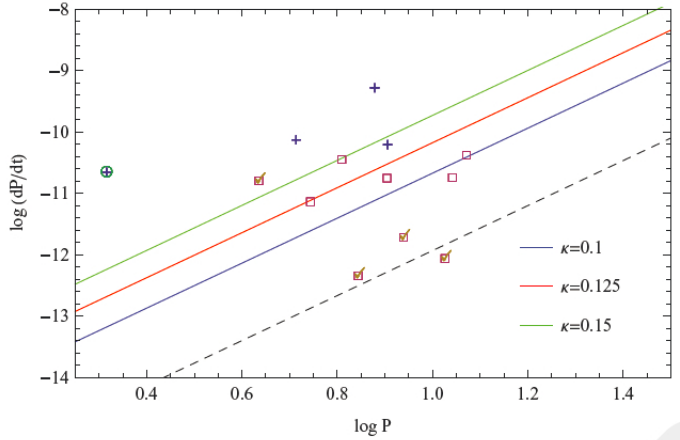

Dependence of death-lines from inclination angle χ

The expression for the death-line of the inclined magnetar is

$$
\begin{aligned}
B \quad > \quad & 2^{-\frac{8}{3}} 3 \xi_{min}^{-\frac{2}{3}} \left\{ \left| \frac{\kappa}{f(1)} \cos\chi (1 - \xi_{min}^2) \right.\right. \\
+ \quad & \left.\left. \frac{3}{4} \frac{1}{(f(1))^{3/2}} \sqrt{\frac{R_s}{R_c}} \left(\frac{\Theta(\eta)}{\Theta_0} - H(1) \right) \sin\chi \right| \right\}^{-1} \left(\frac{P}{1s} \right)^{\frac{7}{3}} \left(\frac{R_s}{10km} \right)^{-3} 10^{12}\mathrm{G} \,.
\end{aligned}
$$

Death-lines for the misaligned magnetar for different values of the inclination angle χ. The value of κ is taken to be 0.1. The dashed line indicates the position of the Newtonian death-line. Crosses and squares indicate the position of SGRs and AXPs, respectively. Anomalous X-ray pulsars from which the radio emission has been registered are marked with ticks, radio-loud soft gamma-ray repeater is enclosed in circle.

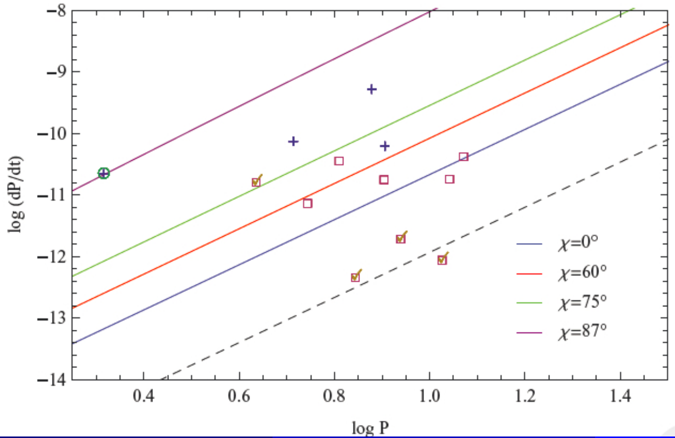

Content

RAGtime 22 online

EM scalar potential

GR EM scalar potential in the polar cap region of rotating and oscillating aligned magnetar magnetosphere is given by

$$\Psi(\theta,\phi)=\frac{B_0}{2}\frac{R_s^3}{R_c^2}\frac{\kappa}{f(1)}\left(1-\xi^2\right)-e^{-i\omega t}\tilde{\eta}(R_s)B_0R_s\sum_{l=0}^{\infty}\sum_{m=-l}^{l}Y_{lm}(\theta,\phi)\ .$$

The condition for radio emission on the intensity of MF is given by

$$\begin{aligned} B &> 2^{-\frac{8}{3}}6\pi\left\{\int_0^{2\pi}\xi_{min}^{2/3}\left|\frac{\kappa}{f(1)}(1-\xi_{min}^2)\right.\right. \\ &- \left.\left.2\frac{\tilde{\eta}(R_s)}{f^m(1)}\left(\frac{R_s}{R_c}\right)^{\frac{m}{2}-2}\xi_{min}^m A_{lm}(\phi)\right|d\phi\right\}^{-1}\times\left(\frac{P}{1s}\right)^{\frac{7}{3}}\left(\frac{R_s}{10km}\right)^{-3}10^{12}\mathrm{G}\ , \end{aligned}$$

in the approximation $Y_{lm}(\theta,\phi)\approx A_{lm}(\phi)\theta^m$ being valid in the limit of small polar angles θ.

Dependence of death-lines from parameter K

The amplitude of the oscillation is now parametrized in terms of the small number $K = \tilde{\eta}(1)/\Omega R$, giving the ratio between the velocity of oscillations and the linear rotational velocity of magnetar. The death-lines for rotating as well as oscillating magnetars for two modes of oscillations and different values of the parameter K are provided.

Death-lines for rotating and oscillating magnetars in the $P - \dot{P}$ diagram. The left panel corresponds to the mode $(1, 1)$ and values of $K = 0\ , 0.01\ , 0.02\ , 0.03$. The right panel corresponds to the mode $(2, 1)$ and values of $K = 0\ , 0.01\ , 0.02\ , 0.03$. Other parameters are taken to be $R_s = 10\mathrm{km}$, $M = 2M_{\odot}$ and $\kappa = 0.15$. Crosses and squares indicate the position of SGRs and AXPs, respectively. AXPs from which the radio emission has been registered are marked with ticks, radio-loud soft gamma-ray repeater is enclosed in circle.

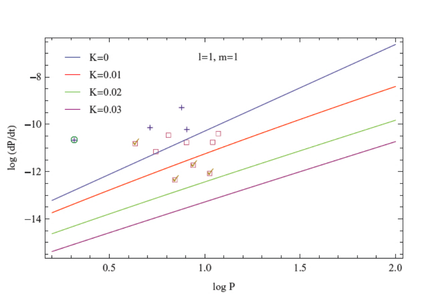

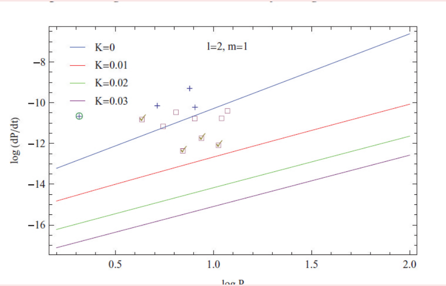

Fast Radio Bursts (FRBs)

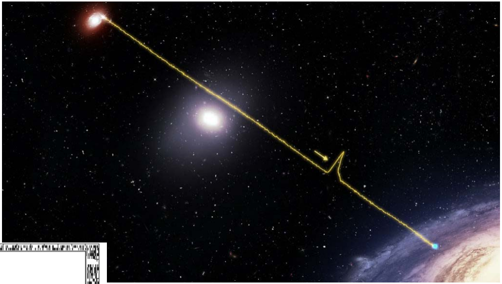

D.Lorimer, D. Narkevic
Nature 2007

"Lorimer" bursts

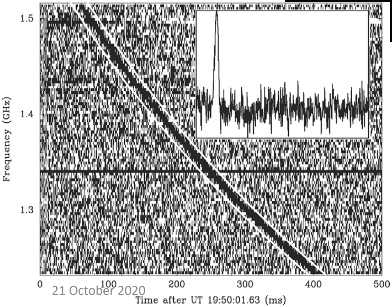

Quasi-periodically Repeating FRBs

K M Raj wade et.al **Possible periodic activity in the repeating FRB 121102, MNRAS 2020**
(P= 10-150 days) 600MHz-8GHz (4÷50 cm)

Periodic activity from a fast radio burst source
(The CHIME/FRB Collaboration*) *Nature* 2020
(P=16.35 ± 0.15 days) 400-800MHz (40÷75cm)

21 October 2020 10

Radiation luminosity

Plasma magnetospheric radiations

Magnetodipolar radiations

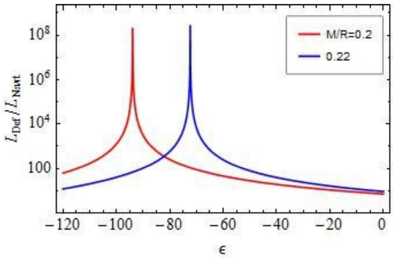

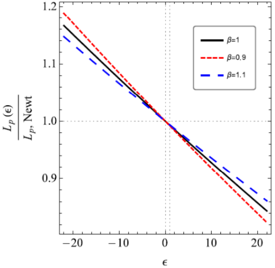

$L_{Newt} \cong 10^{38} erg/sec$
$L_{max} \cong 10^{47} erg/sec$

Wenbin & Kumar, MNRAS Letters, 483,1 (2019)

$L_{max} \cong 2 \times 10^{47} erg/sec$

one may fit the time dependence of the source NS deformation using recorded data of appearance of a repeating FRB

21 October 2020 11

Content

RAGtime 22
online

Dependence of the Lorentz factor on the ratio $j/\bar{j}_*$ for a neutron star with $M = 1.4 M_\odot$, $R = 10$ km, $P = 0.1s$, $\chi = 30°$, $B_0 = 1.0 \times 10^{12}$G, $\theta_* = 0°$, $\Theta_0 = 2°$, $\gamma_* = 1.01$.

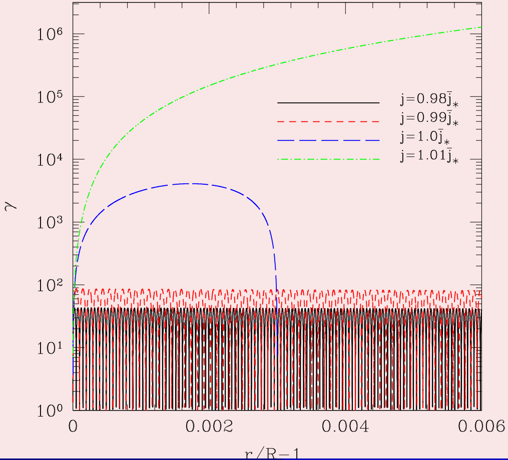

Lorentz factor dependence on the intensity of the magnetic field for a neutron star with $M = 1.4M_{\odot}$, $R = 10$ km, $P = 0.1s$, $\chi = 30°$, $\theta_* = 0°$, $\Theta_0 = 2°$, $\gamma_* = 1.01$. Top panel: $j = 0.98\bar{j}_*$. Bottom panel: $j = 1.01\bar{j}_*$.

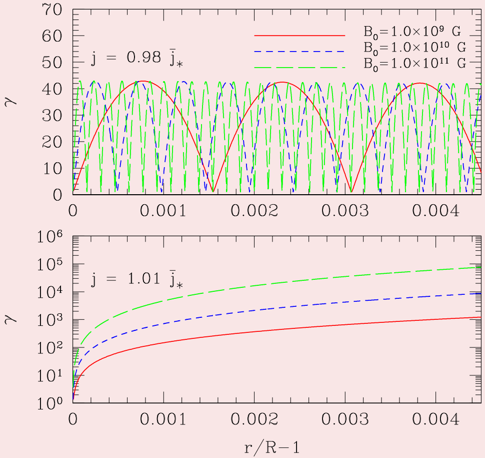

Lorentz factor dependence on the inclination angle χ for a neutron star with $M = 1.4M_\odot$, $R = 10$ km, and $P = 0.1s$, $j = 1.01\bar{j}_*$, $\theta_* = 0°$, $\Theta_0 = 2°$, $\gamma_* = 1.01$, $B_0 = 1.0 \times 10^{12}$G. The Lorentz factor decreases for larger inclination angles.

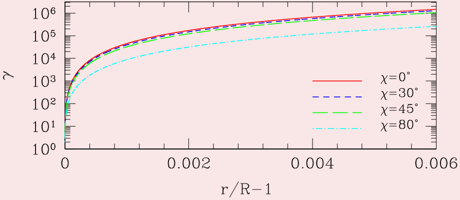

Lorentz factor dependence on the normalized amplitude of the stellar oscillations K for the mode of oscillations $(l, m) = (1, 1)$ with $\theta_* = 2^\circ$, $\Theta_0 = 3^\circ$, $\gamma_* = 1.015$, $B_0 = 1.0 \times 10^{12}$G for the case $j = 0.98\bar{j}_*$. The left panels show the solution for $\phi = 0$, the right panels for $\phi = \pi$.

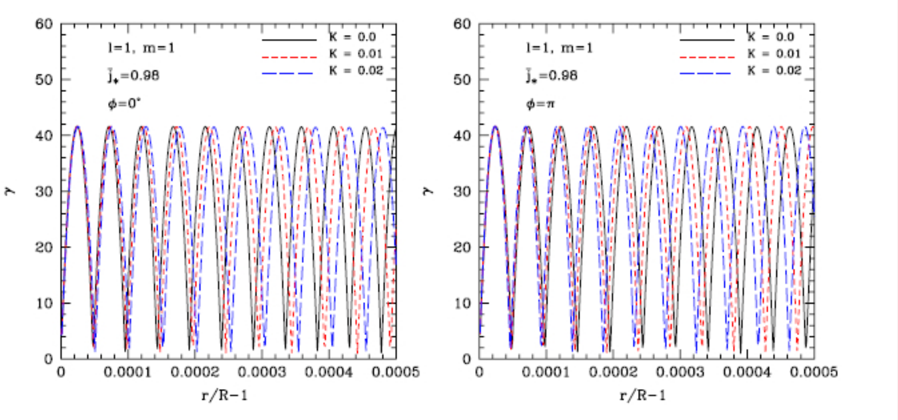

Lorentz factor dependence on the normalized amplitude of the stellar oscillations K for the mode of oscillations $(l, m) = (1, 1)$ with $\theta_* = 2°$, $\Theta_0 = 3°$,$\gamma_* = 1.015$, $B_0 = 1.0 \times 10^{12}$G for the case $j = 1.001\bar{j}_*$. The left panels show the solution for $\phi = 0$, the right panels for $\phi = \pi$.

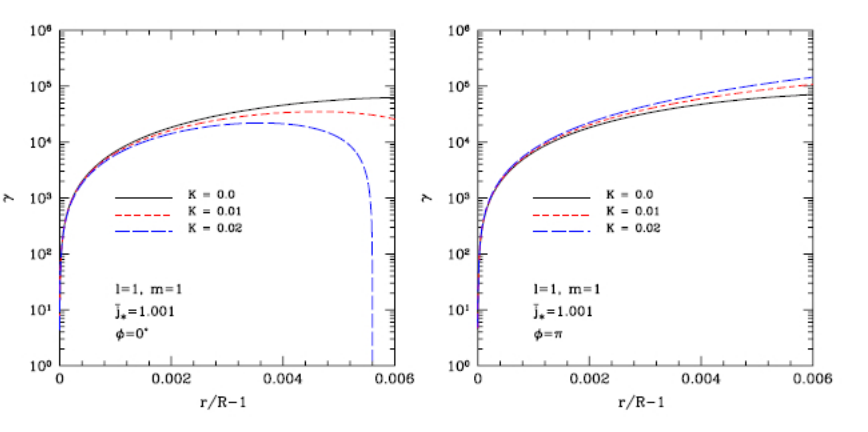

Lorentz factor dependence on the normalized amplitude of the stellar oscillations K for the mode of oscillations $(l,m)=(2,1)$ with $\theta_*=2^\circ$, $\Theta_0=3^\circ$, $\gamma_*=1.015$, $B_0=1.0\times10^{12}$G. The two panels correspond to the case $j=1.001\bar{j}_*$. The left panel shows the solution for $\phi=0$, the right panel for $\phi=\pi$

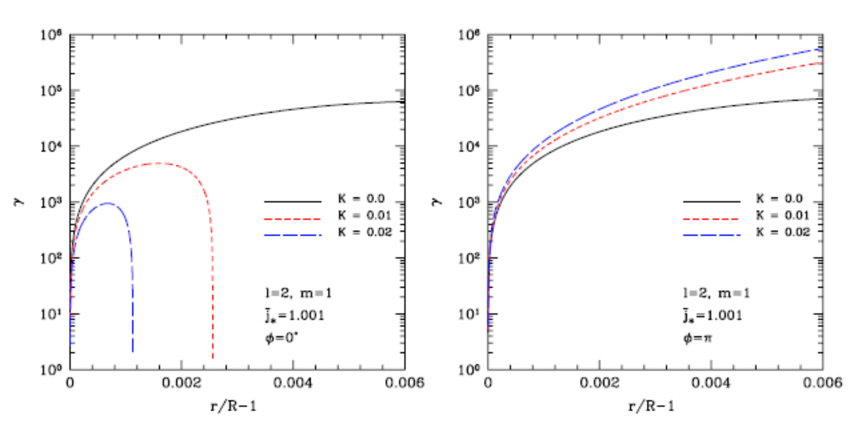

Lorentz factor as a function of radial distance and azimuthal angle ϕ for a model with stellar oscillations $K = 0.02$, $(l, m) = (1, 1)$, $\theta_* = 2°$, $\Theta_0 = 3°$,$\gamma_* = 1.015$, $B_0 = 1.0 \times 10^{12}$G. Left panel: $j = 1.001\bar{j}_*$. Right panel: $j = 1.01\bar{j}_*$.

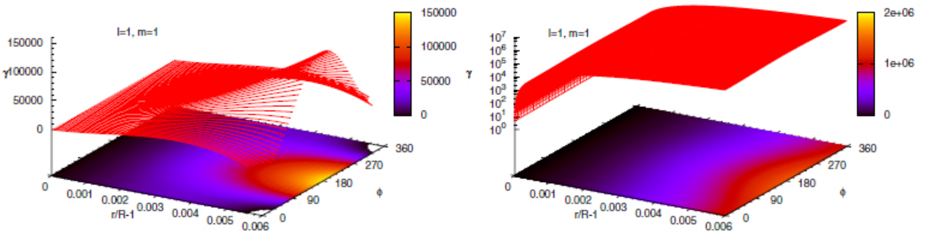

Content

RAGtime 22 online

Drifting Subpulses as a Tool for Studies of Pulsar Magnetosphere

- Phenomena of drifting subpulses
- Existing models for the drifting subpulses
- Our results in frame of the space charge limited flow model

V.S. Morozova, Ahmedov B.J., O. Zanotti, Explaining the subpulse drift velocity of pulsar magnetosphere within the space-charge limited flow model, **MNRAS**, 2014, V. 444, 1144

RAGtime 22 online

Content

Drifting subpulses

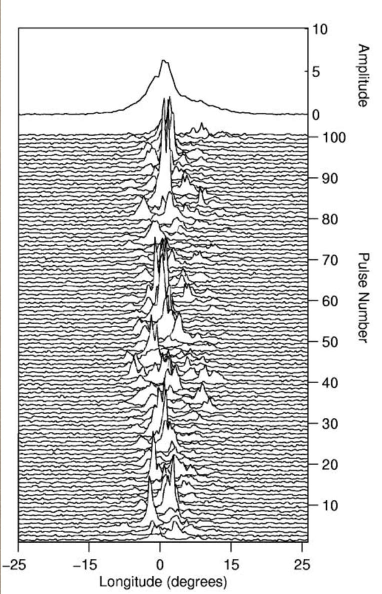

- *Average pulse profile is very stable and represents a unique "fingerprint" of a given pulsar*
- *Subsequent pulses plotted on top of each other show rich microstructure*

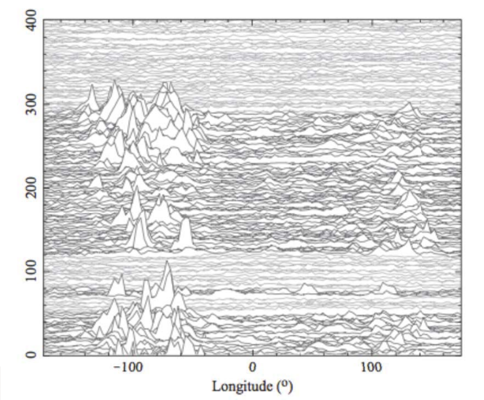

Drifting subpulses

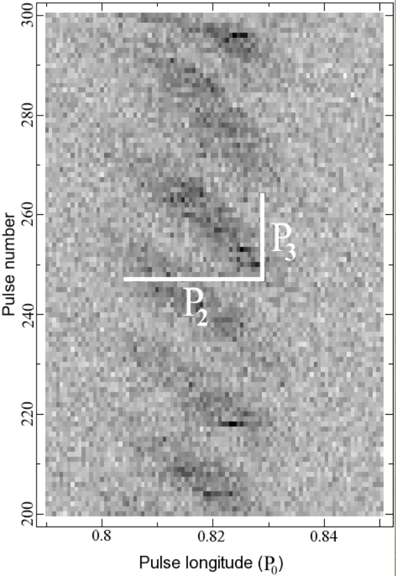

Subpulse drift velocity

$$\omega_D = \frac{P_2}{P_3}$$

Various subpulse behavior

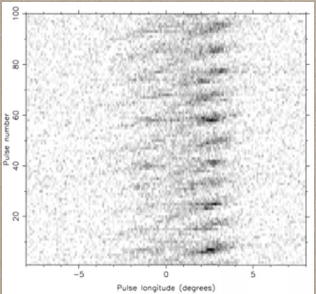

PSR B0320+39 from R. T. Edwards et al. (2003)

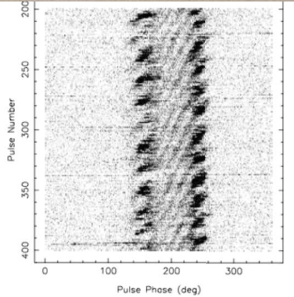

PSR B0818–41 from B. Bhattacharyya et al. (2007)

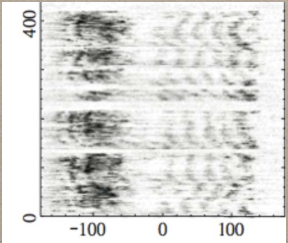

PSR B0826-34 from van Leeuwen & Timokhin (2012)

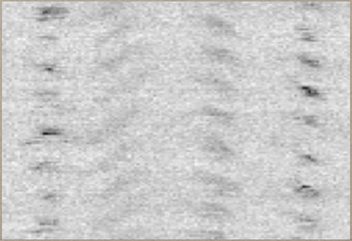

PSR J0815-09 from Qiao et al. (2004)

Content

How many charged particles will actually leave the surface of the star?

A. All required for the screening of the induced electric field

Arons & Scharlemann (1979)

Space-charge limited flow (SCLF) model

B. None

Ruderman & Sutherland (1975)

Vacuum gap model

C. Some part of the amount required for the screening

Gil & Sendyk (2000)

Partially screened gap model

Vacuum gap model

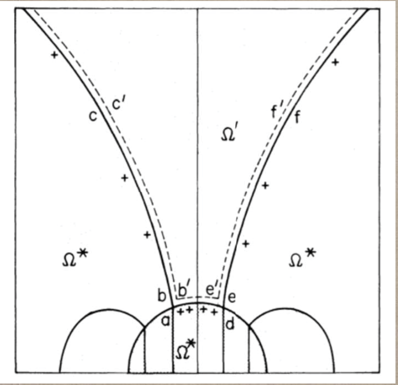

- *A vacuum gap will be formed close to the surface of the star*
- *The gap will periodically discharge in the form of sparks*
- *Sparks are assumed to be responsible for the appearance of the drifting subpulses*

$$\omega_D = \frac{\Delta V}{B_s r_p} c$$

potential drop of the gap

surface magnetic field

radius of the polar cap

Predicted velocities are too large in comparison with the observed

Partially screened gap model

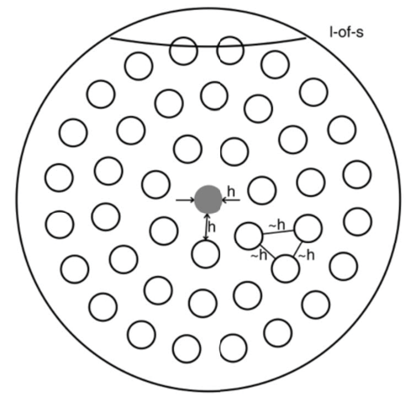

- *Even when the vacuum gap is screened on ~95%, the remaining potential drop is enough for the spark discharges to appear*
- *Sparks are assumed to densely populate the polar cap region*

Predicted velocities can be brought to correspondence with the observed ones, but the degree of screening (shielding factor) is fine tuned and different for different pulsars

Content

RAGtime 22 online

SCLF model

- *Scalar potential is induced due to the difference between the actual charge density in the magnetosphere and the charge density needed to screen the accelerating electric field*

$$\Delta V = -4\pi(\rho - \rho_{GJ})$$

- *Provides analytical solutions for the charge density and electromagnetic field regions close to the surface and far from the surface of the neutron star*

Was never used for the explanation of the drifting sub pulses:

- Potential drop is too small (10^9 V vs 10^{12} V)

- No place for the discharges

van Leeuwen & Timokhin (2012)

$$v_D = \frac{\Delta V}{B_s r_p} c \quad ?$$

$$v = \frac{\vec{E} \times \vec{B}}{B^2} c \qquad \vec{E} = -\nabla V$$

$$\boxed{v_D = \frac{180^\circ}{\xi} \frac{dV}{d\xi}} \qquad \xi \equiv \frac{\theta}{\theta_{pc}}$$

The drift velocity is defined by the shape of the potential, not by its absolute value

What if we try to check the SCLF model?

Expression for the plasma velocity

$$\omega_{D\ \rm low} = \frac{180^\circ}{\xi}\frac{12\sqrt{1-\varepsilon}\Theta_0}{\bar{r}}\left\{-2\kappa\cos\chi\sum_{i=1}^{\infty}\left[\exp\left(\frac{k_i(1-\bar{r})}{\Theta_0\sqrt{1-\varepsilon}}\right)-1+\frac{k_i(\bar{r}-1)}{\Theta_0\sqrt{1-\varepsilon}}\right]\frac{J_1(k_i\xi)}{k_i^3 J_1(k_i)}\right.$$
$$\left.+\Theta_0 H(1)\delta(1)\sin\chi\cos\phi\sum_{i=1}^{\infty}\left[\exp\left(\frac{\tilde{k}_i(1-\bar{r})}{\Theta_0\sqrt{1-\varepsilon}}\right)-1+\frac{\tilde{k}_i(\bar{r}-1)}{\Theta_0\sqrt{1-\varepsilon}}\right]\frac{J_0(\tilde{k}_i\xi)-J_2(\tilde{k}_i\xi)}{2\tilde{k}_i^3 J_2(\tilde{k}_i)}\right\}$$

$\bar{r}\equiv\frac{r}{R}$ $\quad\xi\equiv\frac{\theta}{\theta_{pc}}$ $\quad\phi$ *- spherical coordinates*

- *Are the values of drift velocity predicted by this expression compatible with the observed subpulse velocities?*
- *May the angular dependence of the drift velocity help in explaining the longitudinal subpulse behavior?*

Comparison with the pulsar data

- *Weltevrede et al. (2006), (2007) did the first systematic study of the subpulse behavior of large amount of pulsars (at 21 cm and 92 cm observational wavelength)*
- *From 187 pulsars more than 55 % show the subpulse phenomena (revealed by the spectral methods)*
- *We chose 13 pulsars with known observing geometry (the inclination angle χ)*

$$\omega_D = \omega_D(\bar{r}, \xi, \phi) \qquad \xi = 0.9\,, \;\; \phi = \pi$$

Find $\bar{r}$ **so that** $\omega_D(\bar{r}) = \omega_{observed}$

- *One pulsar does not have a solution, one has the opposite drift sense at two observing frequencies*

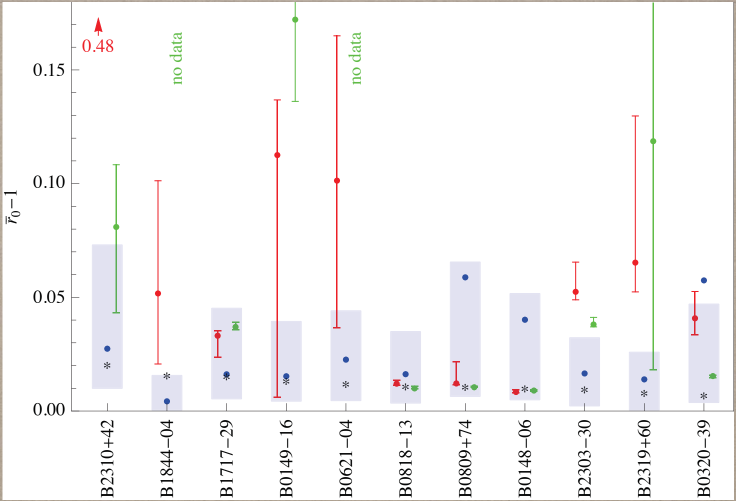

Red data points correspond to the observing wavelength at 21 cm

Green data points correspond to the observing wavelength at 92 cm

Blue shadowed rectangles and blue points indicate the pair formation front (PFF)

Pair formation front

- *Primary particles, emitted from the surface, accelerate in the inner magnetosphere and emit high energy gamma photons via:*

  - Curvature radiation

  - Inverse Compton scattering

- *Emitted gamma photons produce electron-positron pairs in the background magnetic field*

- *Pair production leads to the screening of the accelerating electric field and prevents further acceleration above the pair formation front*

PSR B0826-34

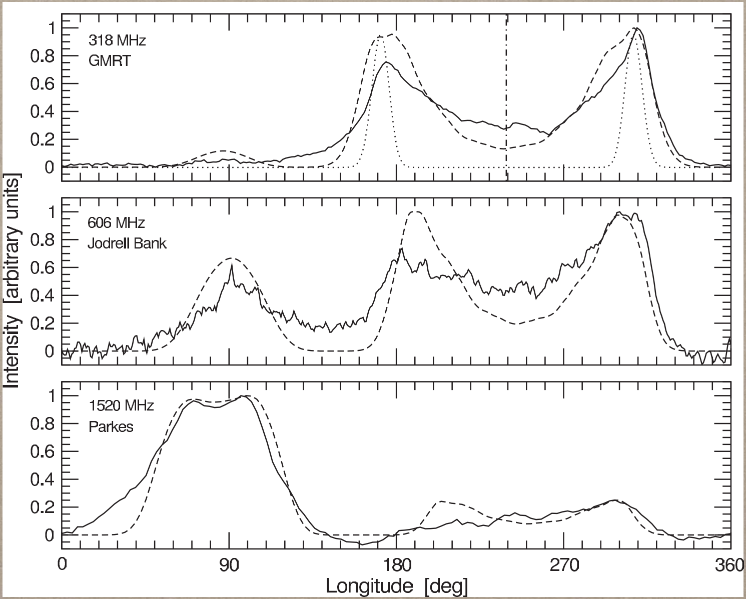
318 MHz
GMRT
606 MHz
Jodrell Bank
1520 MHz
Parkes
Intensity [arbitrary units]
Longitude [deg]
0
0.2
0.4
0.6
0.8
1
0
90
180
270
360

PSR B0826-34

Observing frequency (MHz)	Measured drift velocity ($^\circ/P$)	Reference	Average drift velocity ($^\circ/P$)
318	$-0.8 \div 1.9$	Gupta et al. (2004)	0.55
645	$-1.5 \div 2.1$	Biggs et al. (1985)	0.3
1374	$-3.2 \div 3.6$	Esamdin et al. (2005)	0.2
1374	$-1 \div 1.5$	van Leeuwen & Timokhin (2012)	0.25

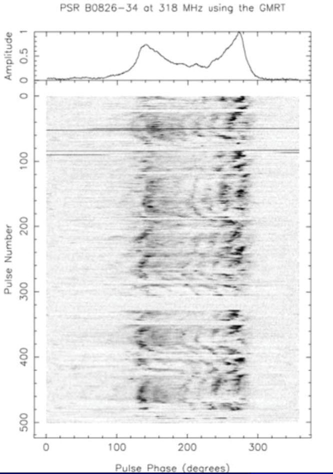

Measured subpulse separation

$$P_2 = 24.9^\circ \pm 0.8^\circ$$

The pulsar is almost aligned, our model predicts negative drift velocity

What if the positive average drift is only apparent?

$$\omega_D = (0.55^\circ - 24.9^\circ)/P = -24.35^\circ ?$$

$$P_3 \approx P \quad ?$$

Our model for the observing geometry

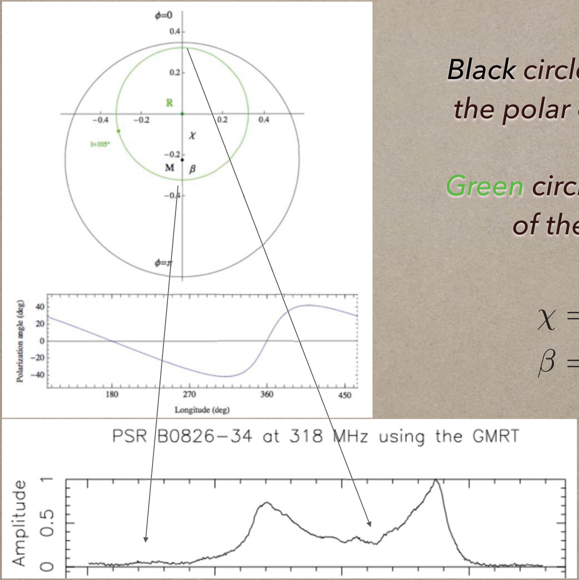

Black circle - boundary of the polar cap (0.57 deg)

Green circle - line of sight of the observer

$$\chi = 0.225^\circ$$
$$\beta = 0.098^\circ$$

Consistent with the polarization data and with the width of the profile

Explaining the range of measured velocities

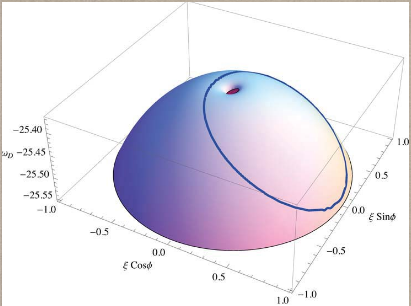

- *Plasma drift velocity across the pulsar polar cap in the SCLF model*

$$\vec{\omega}_{proj} = \frac{\vec{\omega}}{\sqrt{1+\left(\frac{d\xi}{d\phi}\right)^2}}$$

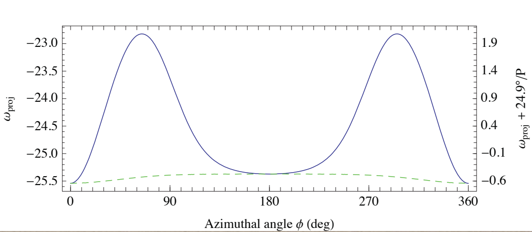

Explaining the longitudinal dependence of subpulse separation

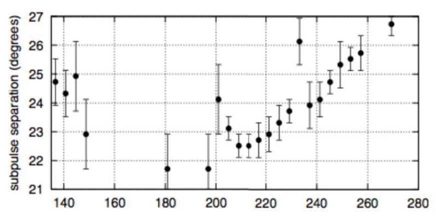

Measured subpulse separation of B0826-34 from Gupta et al. (2004)

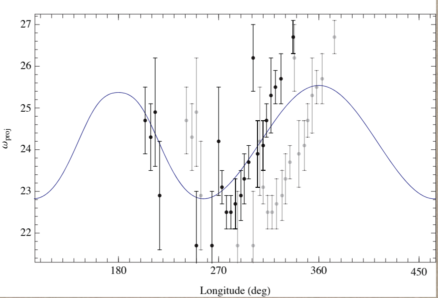

Black points represent the observed data (given in gray), shifted in order to get the visual correspondence

PSR B0818-41

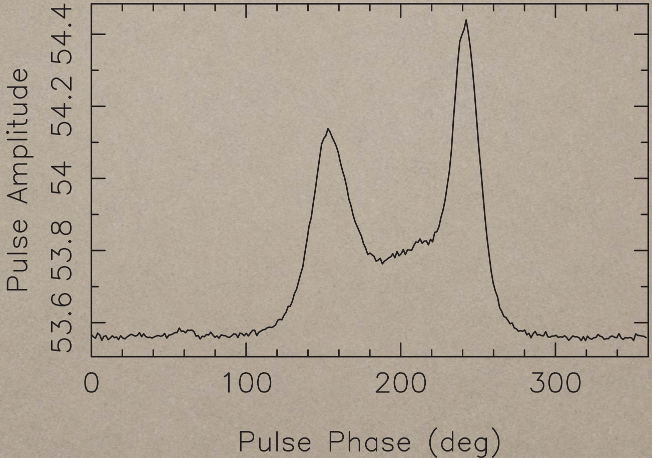

$P = 0.545$ sec $\quad B_s = 1.03 \times 10^{11}$ G

Our model for the observing geometry

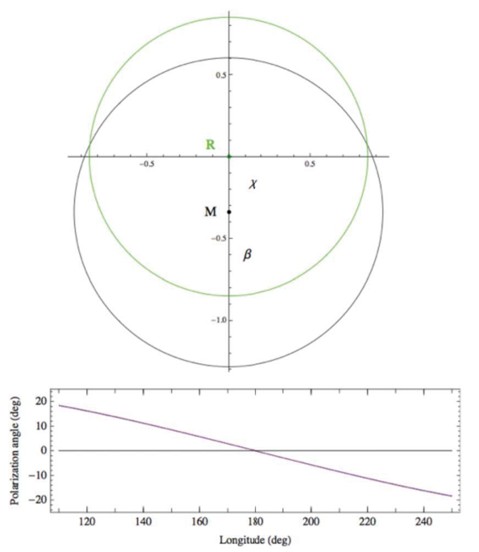

Consistent with the polarization data and with the width of the profile

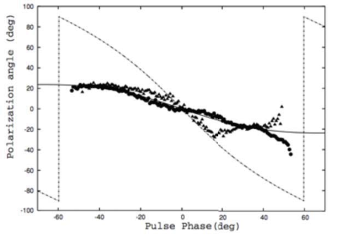

from Bhattacharyya et al. (2009)

Angular dependence of the drift velocity can account for the curved subpulse drift bands of B0818-41

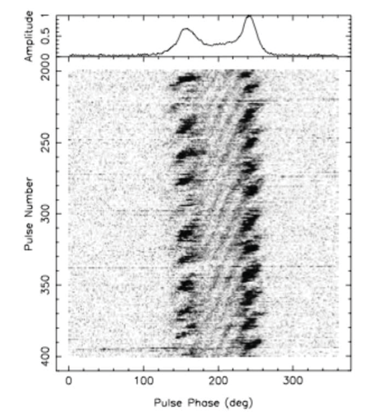

from Bhattacharyya et al. (2009)

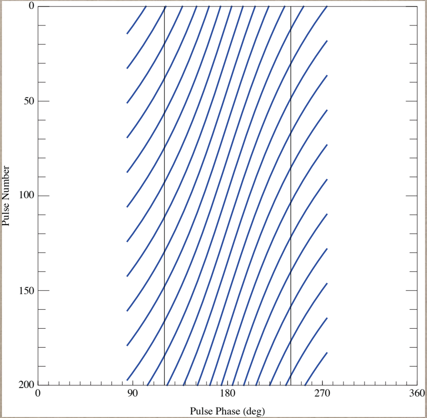

obtained with our model

Content

RAGtime 22 online

Conclusion

- The dependence for the energy losses on the oscillating behavior reflects in useful relation between the product $P\dot{P}$ and the amplitude of the stellar oscillation.
- A connection between the phenomenology of intermittent pulsars, characterized by the periodic transition from active to dead periods of radio emission in few observed sources, with the presence of an oscillating magnetosphere. During the active state, star oscillations may create relativistic wind of charged particles by virtue of the additional accelerating electric field. After a timescale of the order of tens of days stellar oscillations are damped, and the pulsar shifts below the death line in the $P-B$ diagram, thus entering the OFF invisible state of intermittent pulsars.

Conclusion

- **The dependence for the energy losses on the oscillating behavior reflects in useful relation between the product $P\dot{P}$ and the amplitude of the stellar oscillation.**
- **A connection between the phenomenology of intermittent pulsars, characterized by the periodic transition from active to dead periods of radio emission in few observed sources, with the presence of an oscillating magnetosphere. During the active state, star oscillations may create relativistic wind of charged particles by virtue of the additional accelerating electric field. After a timescale of the order of tens of days stellar oscillations are damped, and the pulsar shifts below the death line in the $P-B$ diagram, thus entering the OFF invisible state of intermittent pulsars.**

Conclusion

- A detailed analysis of the position of the death-line in the $P-\dot{P}$ diagram for a magnetar is performed. When the compactness of the neutron star is increased, the death line shifts upwards in the $P-\dot{P}$ diagram, pushing the magnetar in the radio-quiet region.
- When the inclination angle χ between the angular momentum vector and magnetic moment is increased, the death-line shifts upwards in the $P-\dot{P}$ diagram, pushing the magnetar in the radioquiet region.
- Larger compactness parameters of the star as well as larger inclination angles between the rotation axis and the magnetic moment produce death-lines well above the majority of known magnetars. This is consistent with the observational evidence of no regular radio emission from the magnetars in the frequency range typical for the ordinary pulsars.

Conclusion

- A detailed analysis of the position of the death-line in the $P - \dot{P}$ diagram for a magnetar is performed. When the compactness of the neutron star is increased, the death line shifts upwards in the $P - \dot{P}$ diagram, pushing the magnetar in the radio-quiet region.
- When the inclination angle χ between the angular momentum vector and magnetic moment is increased, the death-line shifts upwards in the $P - \dot{P}$ diagram, pushing the magnetar in the radioquiet region.
- Larger compactness parameters of the star as well as larger inclination angles between the rotation axis and the magnetic moment produce death-lines well above the majority of known magnetars. This is consistent with the observational evidence of no regular radio emission from the magnetars in the frequency range typical for the ordinary pulsars.

Conclusion

- **A detailed analysis of the position of the death-line in the $P - \dot{P}$ diagram for a magnetar is performed. When the compactness of the neutron star is increased, the death line shifts upwards in the $P - \dot{P}$ diagram, pushing the magnetar in the radio-quiet region.**
- **When the inclination angle χ between the angular momentum vector and magnetic moment is increased, the death-line shifts upwards in the $P - \dot{P}$ diagram, pushing the magnetar in the radioquiet region.**
- **Larger compactness parameters of the star as well as larger inclination angles between the rotation axis and the magnetic moment produce death-lines well above the majority of known magnetars. This is consistent with the observational evidence of no regular radio emission from the magnetars in the frequency range typical for the ordinary pulsars.**

Conclusion

- **The SCLF model predicts the subpulse drift velocities compatible to the observed ones at heights above the surface of the star close to the pair formation front**
- **The angular dependence of the plasma drift velocity in the SCLF model provides a natural explanation for the variation of the subpulse separation along the pulse**
- **In particular it may explain the curved subpulse driftbands of PSR B0818-41 and the range of the observed drift velocities of PSR B0826-34**

Conclusion

- **The SCLF model predicts the subpulse drift velocities compatible to the observed ones at heights above the surface of the star close to the pair formation front**
- **The angular dependence of the plasma drift velocity in the SCLF model provides a natural explanation for the variation of the subpulse separation along the pulse**
- **In particular it may explain the curved subpulse driftbands of PSR B0818-41 and the range of the observed drift velocities of PSR B0826-34**

Conclusion

- The SCLF model predicts the subpulse drift velocities compatible to the observed ones at heights above the surface of the star close to the pair formation front
- The angular dependence of the plasma drift velocity in the SCLF model provides a natural explanation for the variation of the subpulse separation along the pulse
- In particular it may explain the curved subpulse driftbands of PSR B0818-41 and the range of the observed drift velocities of PSR B0826-34

Thank You